Nanoscale

COMMUNICATION

Cite this: *Nanoscale*, 2017, **9**, 1428

Received 26th September 2016,
Accepted 18th December 2016

DOI: 10.1039/c6nr07602e

www.rsc.org/nanoscale

A composite generator film impregnated with cellulose nanocrystals for enhanced triboelectric performance†

Jun Peng,[a,b] Huilong Zhang,[c] Qifeng Zheng,[d] Craig M. Clemons,[e] Ronald C. Sabo,[e] Shaoqin Gong,[d] Zhenqiang Ma[c] and Lih-Sheng Turng*[a,b]

A novel polydimethylsiloxane (PDMS)/cellulose nanocrystal flake (CNCF) composite triboelectric nanogenerator (CTG) using CNCFs as effective dielectrics exhibited a 10-times-enhanced triboelectric performance compared with its pure PDMS counterpart. Positive charges generated on the surface of the CNCFs during cyclic compression boosted electron transfer and induced extra charges. The CTG exhibited an instantaneous output power (density) of 1.65 mW (0.76 mW cm^{-2}) under continuous operation.

Introduction

Triboelectric nanogenerators (TENGs) are emerging devices used to scavenge mechanical energy from an ambient environment to produce electricity using functional nanomaterials.[1–6] TENGs have been developed based on triboelectric charge (contact charge) generation and electrostatic induction effects.[7–10] Rubbing or pressing together two dissimilar materials can generate contact charges on their surfaces, known as contact electrification.[11] Contact charging between metal–metal contacts is well understood by electron exchange theory. The different surface energy levels (*i.e.*, work functions)[12] act as the driving force for electron transfer. Electric charge generation between metal–insulator contacts is attributed to the ion exchange mechanism when mobile ions are present as carriers. Given no electrons or ions for the identical insulator–insulator, material transfer is hypothesized to occur during the contact charging process.[13–15] To pursue high output power, TENGs have been recently designed and investigated employing metal–insulator or insulator–insulator contacts to generate triboelectric charges. Materials and structures are two critical factors for enhancing triboelectric performance.

Harnessing the superior mechanical and electromechanical properties of nanoscale structures, TENGs can be used to harvest energy from rotating friction,[16,17] fluid or air flow,[18–20] human activities,[21,22] and even wearable clothing.[23] To date, the output power of TENGs has reached the milliwatt per cm^2 level,[24] which is sufficient to power many small electronic devices such as light-emitting diodes (LEDs),[25] temperature sensors,[26] displacement sensors,[27] and several chemical and solvent vapor detectors.[20,28,29] To enhance the electrical performance, work has been done to increase the effective friction by creating nanopatterns or nanofeatures on the film surface,[7,30] or by introducing multi-scale porous voids inside of polydimethylsiloxane (PDMS).[31] Chemical surface functionalization on contact surfaces indicates the potential to enhance the surface charge density.[32,33] Furthermore, another promising strategy to enhance the triboelectric performance is to employ various kinds of conductive nanoparticles or nanowires dispersed in dielectric PDMS.[34,35] However, most TENGs require sophisticated surface patterns and nanostructure designs to attain high performance. Also, due to the soft and ductile behavior of nanoparticles/nanowires, the performance of TENGs decreases with their use, or when they encounter a large applied pressure. Therefore, output power stability remains an elusive goal.

Moreover, the fabrication of many TENGs using fillers as dielectrics involves the consumption of precious materials (*e.g.*, gold (Au) nanoparticles and carbon nanotubes). Therefore, the realization of triboelectric generators based on biodegradable and biorenewable cellulose nanocrystals isolated from abundant natural cellulose is highly desired.

A novel biorenewable cellulose composite triboelectric generator (CTG) with a stable power output performance has been developed. The CGT contains cellulose nanocrystal flakes (CNCFs) directionally embedded in the PDMS film and aluminum (Al) film electrodes. The open-circuit voltage and

[a]*Polymer Engineering Center, University of Wisconsin–Madison, Madison, Wisconsin 53706, USA. E-mail: turng@engr.wisc.edu*
[b]*Wisconsin Institute for Discovery, University of Wisconsin–Madison, Madison, Wisconsin 53715, USA*
[c]*Department of Electrical and Computer Engineering, University of Wisconsin–Madison, Madison, Wisconsin 53706, USA*
[d]*Department of Materials Science and Engineering, University of Wisconsin–Madison, Madison, Wisconsin 53706, USA*
[e]*USDA Forest Service, Forest Products Laboratory, Madison, Wisconsin, 53726, USA*
†Electronic supplementary information (ESI) available. See DOI: 10.1039/c6nr07602e

short-circuit current density from the CTGs achieved high values of ~350 V and ~5 μA cm^{-2}, respectively, which gave a 10-fold power increase compared with pure PDMS TENGs under the same periodic compression. This simple and scalable CTG technique provides a promising solution for large-scale power generation and self-powered electronic devices. In this study, CTGs with various concentrations of oriented CNCFs were fabricated and the test results showed that the output performance was affected by the compressive pressure, filler concentration, and surface charge density.

Results and discussion

A schematic illustration of the fabrication and microstructures of cellulose composite triboelectric generators (CTGs) is shown in Fig. 1. The cellulose nanocrystal flakes (CNCFs) were produced by the wet ball milling and freeze drying processes, and the composite-structured PDMS/CNCF films were fabricated by spin coating (see the ESI† for fabrication details). The CNCFs were oriented parallel to the PDMS surface due to the shear flow and thinning of the film thickness from centrifuging. CNCFs had a uniform dispersion in the PDMS film and formed a non-continuous layered structure, as shown in the SEM image in Fig. 1(b), which is the cross-section of the composite film. The nanostructure of cellulose nanocrystals and corresponding morphologies of the composite-structured films with various CNCF concentrations are shown in the ESI, Fig. S1.† The construction of a CTG is fairly straightforward. Aluminum tape as the bottom electrode was directly attached to one surface of the PDMS without an adhesive layer. Kapton tape was used as an insulator for the top and bottom Al electrodes (see Fig. S2† for the components and testing setup). The pressing frequency and separation gap were adjusted by a programmed solenoid. As paired pressing materials, Al and PDMS exhibited the opposite polarities,[7] while cellulose possessed a positive polarity.[36] In order to compare the output performance and illustrate the benefits of CNCF-filled CTGs, a TENG using a pure PDMS film with the same thickness was fabricated as a reference.

Fig. 2(a) and (b) show the open-circuit voltage and short-circuit current density between the two electrodes—which were generated by TENGs based on a pure PDMS film and CTGs with 2.5 wt% CNCFs—under a periodic compressive force of 40 N (corresponding to a compressive pressure of 0.18 MPa) at a constant frequency of 10 Hz. The oscillating output current was attributed to induced charges transferring through an external load during the periodic change in the separation distance. Current or induced charges were driven by the accumulated electrons on the PDMS surface after contact charging between the metal and insulator.[14,15,37,38] The output voltage and current density increased with the addition of CNCFs. The CTGs had record peak values of open-circuit voltage and short-circuit current density of 320 V and 5 μA cm^{-2}, respectively, which were 2 to 4 times higher than that of TENGs under the same compressive force.

The current flow of induced charges through an external circuit is schematically illustrated in Fig. 2(c) over one compression cycle. At the initial state, the top Al electrode and the PDMS film were separated, thus there were no transferred charges and no potential difference. When an external force drove the top Al film to be in contact with the PDMS film to induce contact charging through rubbing and pressing, electron transfer occurred from the top Al electrode to the contacted PDMS side, leading to negative triboelectric charges on the PDMS surface and positive charges on the top Al electrode. Upon the release of the compression force, the top Al electrode had a higher potential as compared to the bottom

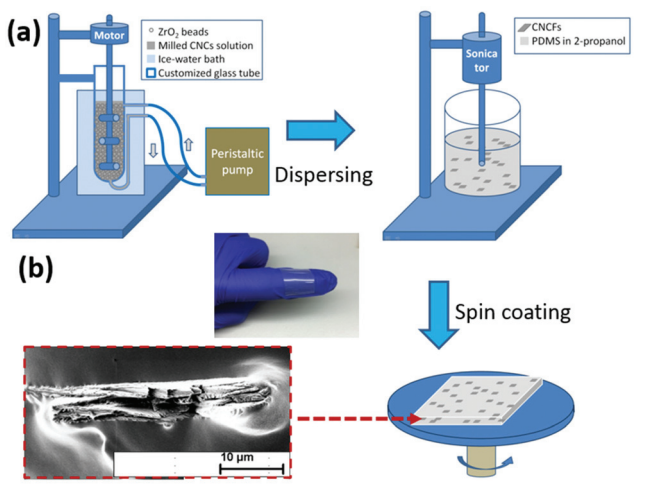

Fig. 1 (a) Illustrations of the production of CNCFs following the ball milling, sonication, and spin coating processes. (b) A small piece of the as-fabricated PDMS/CNCFs2.5 film adhered to the surface of a glove and an SEM image of oriented CNCFs.

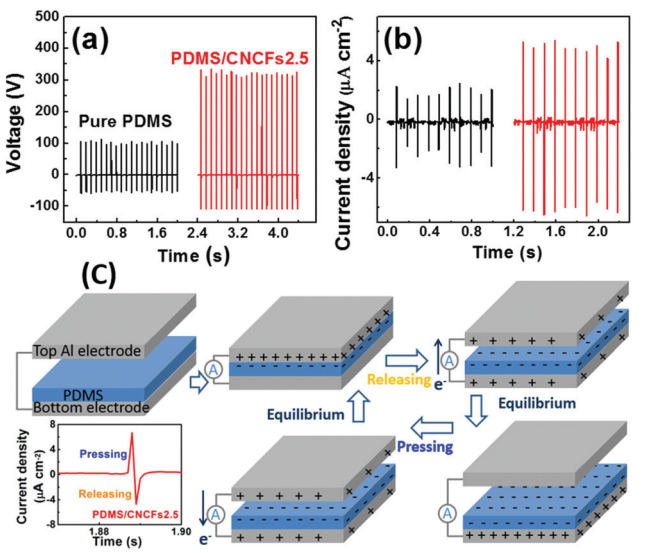

Fig. 2 Electrical output performance: (a) open-circuit voltage and (b) short-circuit current density of a TENG and CTG with 2.5 wt% CNCFs. (c) Schematic images of an induced charge current flow through an external circuit over a compression cycle.

one. Thus, the electrons began to transfer to the top Al electrode through the external circuit to neutralize the positive triboelectric charges, resulting in the experimentally observed electric current. During the separation stage, the total charges on the top and bottom Al electrodes redistributed depending on the distance between the top Al electrode and the PDMS film (see the ESI, eqn. (S4) and (S5)†). The electrons transferred from the bottom Al electrode to the top Al electrode until reaching an electrostatic equilibrium. This was the first half of the triboelectric charge cycle. Once the TENG was compressed again, the electrostatic equilibrium was broken, and electrons flowed back from the top electrode to the bottom electrode until reaching a new equilibrium. At this stage, the opposite current was detected. This was the second half of the triboelectric charge cycle. According to the test results, the pressing stage occurred prior to the releasing stage, and the magnified plot of the current density changed over one compression cycle (see Fig. 2(c)), illustrating the peak values respectively attributed to the pressing and releasing stages. The average surface charge densities of the pure PDMS and composite with 2.5 wt% CNCFs were ~17 μC m^{-2} and ~60 μC m^{-2}, respectively, which were calculated based on the integral of the short-circuit current output curve.

The charging stage and the electrical outputs depended on the compressive force. The effect of the compressive force on the electric output was investigated. As shown in Fig. 3(a), the open-circuit voltages of the TENGs and CTGs increased with increasing compressive force. This could be attributed to a higher compressive force enlarging the friction (contact) area between the top electrode and the PDMS.

To investigate the effects of dielectric CNCF fillers, the electric outputs of CTGs with CNCF concentrations of 1.0, 2.5, and 5.0 wt% were measured under various compressive forces. For CTGs with 2.5 wt% CNCFs, the maximum recorded voltages were about 210 V and 320 ± 20 V at 20 N and 40 N, respectively, which is almost three to four times higher than that of pure PDMS under the same force range, as shown in Fig. 3(a). When the CNCF concentrations increased to 5 wt%, the high filler content started to cause clusters or agglomerates as detected by SEM images (Fig. S1(h)†), and the output performance decreased.

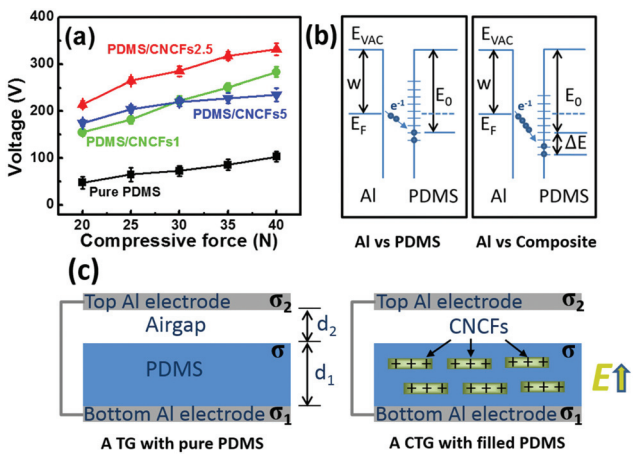

Fig. 3 (a) The electrical output voltages increased with additional CNCF concentrations and compressive testing force. (b) Energy band diagrams indicated the increased probability of electron transfer and surface charge density due to the induced electric field. (c) Illustration of the triboelectric contact electrification processes with the net electric field *E* in composite films along the direction from the PDMS to the top Al electrode; the triboelectric charge transferred to the PDMS surface with a density of σ; and the induced charge density of σ_1 and σ_2.

The surface charge on the insulator is a critical material property that affects the electrical output of a triboelectric generator. A larger value of the surface charge density (σ) of the PDMS can induce a higher surface charge density (σ_1) on the bottom Al electrode, leading to an increase in the output voltage and current density, as shown in eqn (S3) and (S4).† Therefore, the enhancement of the surface charge density and electrical output may be attributed to more electrons being transferred and accumulated on the PDMS surface with the presence of CNCFs.

According to the electron exchange mechanism, the probability of charge transfer between adjacent metal–metal or metal–insulator materials is a function of the surface potential level of the paired materials as characterized by the difference of effective work functions.[39–42] As illustrated by a simplified band diagram in Fig. 3(b), the surface energy state of pure PDMS was indicated by a characteristic energy level (E_0), which is normally lower than the work function of Al (W). The contact charging process occurred after contact between the metal electrode and the insulator, and electrons tended to flow from the filled Fermi level (E_F) of Al into the empty surface states of the PDMS, leaving the PDMS negatively charged. For the composite PDMS films, the impregnated CNCFs exhibited a positive polarity.[36] Also, the CNCFs produced in this study were more positively charged due to the presence of sodium ions during the cellulose nanocrystal acid hydrolysis process and the neutralization that followed. Note that the sodium ions were encapsulated in the PDMS and thus could not be transferred to the PDMS surface. Thus, the charging mechanism was dominated by electron exchange rather than ion exchange. These positively charged CNCFs produced a net electric field (ΔE) along the direction from the PDMS to the top electrode, as shown in Fig. 3(c). This external field increased the potential difference with respect to the Fermi level of the contacted metal, and drove more electrons to be transferred to the PDMS. With the assumption of no leakage, the transferred surface charge density (σ) on the PDMS surface was defined as,

$$\sigma = \frac{\Delta E d_2 + [(W - E_0)/e](1 + d_1/\varepsilon_{rp} d_2)}{d_1/\varepsilon_0 \varepsilon_{rp} + (1/\overline{N_s(E)}e^2)(1 + d_1/\varepsilon_{rp} d_2)}$$

where $W - E_0$ is the difference of effective work function; e, d_2, d_1, ε_{rp}, ε_0, and $\overline{N_s(E)}_s$ are the elementary charge, separation air gap, thickness of PDMS, relative permittivity of PDMS, vacuum permittivity, and average surface density of state, respectively.[43,44] Here, σ increased with ΔE and the CNCF

concentration as well, but a higher concentration (*i.e.*, 5 wt%) caused agglomeration which decreased the σ value. Comparable cases were reported where the external bias voltage[44] and triboelectric positive metal charges[35] were able to induce an extra field to foster electron transfer. Thus, it is believed that the enhanced charge transfer and surface charge density were due to the electric field generated by the presence of CNCFs, as shown in Fig. 3(b) and (c).

A triboelectric generator based on perpendicular contact–separation mode has a layered structure similar to a parallel plate capacitor. The higher value of capacitance corresponds to a larger capacity to store charges and a higher surface charge density accumulation on the dielectric surface. The capacitance ($\varepsilon_0\varepsilon_{rp}S/d$) of the viscoelastic insulator is proportional to the dielectric constant (ε_{rp}) and surface area (S), and inversely proportional to the thickness (d). CNCFs as dielectric fillers possessed a higher dielectric constant (ε_{rp} = 5.2) than the PDMS (ε_{rp} = 2.6), and thus the composite PDMS films impregnated with oriented CNCFs exhibited a higher dielectric constant compared with pure PDMS, as shown in Fig. S3.† In addition, the composite films with small amounts of CNCFs (*i.e.*, 1 or 2.5 wt%) had a lower modulus and were more flexible, as shown in Fig. S4(a) and (b).† Computer simulation (using SolidWorks software) confirmed that the displacement increased with the addition of 2.5 wt% CNCF fillers under a normal force of 20–40 N (see Fig. S4(c)†). Combining the thickness variation due to the compressive force and the increased capacitance of the composite films, the CTGs produced almost 1.5 times improvement in both voltage and current density generation as compared to the TENGs (see Fig. S3†).

To investigate the output power and energy conversion efficiency of CTGs quantitatively, resistors with resistance values of 100 Ω–50 MΩ were connected as external loads. As demonstrated in Fig. 4(a), the instantaneous power output (see eqn (S6)†) depends on the load resistances and CNCF concentrations. Furthermore, the current density drops with increasing load resistance according to Ohm's law. Meanwhile, the voltage increases, leading to the maximum power at a load resistance of 10 MΩ. With an applied normal force of 40 N, a power of 1.65 mW was achieved (Fig. 4(a)), corresponding to a power density of 0.76 mW cm^{-2} for CTGs of a composite PDMS/CNCFs2.5 film, which was more than 10 times that of TENGs of a pure PDMS film (0.06 mW cm^{-2}). This value is substantially larger than the ones previously demonstrated by triboelectric generators.[31,35] The output powers under various applied normal forces are shown in Fig. S5.†

The energy conversion efficiency—an important figure of merit for CTGs—was calculated and is shown in Fig. 4(b). Conversion efficiency is defined as the ratio between the electrical output power that is delivered to the load by CTGs and the total input power mainly containing the mechanical energy to compress the composite film and the power required to separate and compress the top Al electrode to overcome the coulomb attraction force. Fig. S6† shows that the output voltage peaks and duration time of the TENGs and CTGs match well in a single cycle of compression, and that the areas under the curves can be used for the power and energy conversion calculations. The electrical energy power delivered by the CTGs is equal to the joule heating energy over time on the external load of resistance; the calculations are shown in the ESI, eqn. (S7)–(S9).† With the assumption that the effective input mechanical energy alone causes film deformation and overcomes the coulomb force (*i.e.*, without internal friction or heat loss caused by the solenoid), the energy conversion depends on the load resistance and compressive force. Under an applied compressive force of 40 N, the maximum efficiency value of CTGs (PDMS/CNCFs2.5) was ~17% at an external resistance of 10 MΩ.

The superior power output of the CTGs has the potential to power a tremendous number of applications. Here we directly illuminated LEDs in series connected to the CTG. In the case of 40 N, the output power from the CTG (PDMS/CNCFs2.5) without an external load resistor could light up 100 LEDs, while that of the TENG (pure PDMS) was only sufficient to power 30 LEDs under the same compressive force, as shown in Fig. 4(a). This confirms that the PDMS/CNCF composite can dramatically enhance the performance of CTGs.

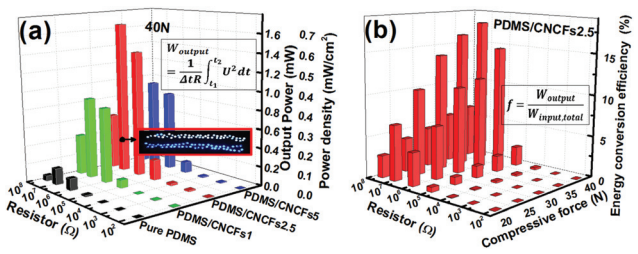

Fig. 4 (a) Dependence of instantaneous output power on the external load resistance (testing range 100 Ω–50 MΩ) under a periodic contact force of 40 N, indicating a maximum power output with a load resistance of 10 MΩ. Snapshots of 100 commercial LEDs connected in series powered by CTG (PDMS/CNCFs2.5). (b) Dependence of energy conversion efficiency on the load resistance and cyclic compressive force.

Conclusion

In conclusion, we demonstrated a novel composite film impregnated with oriented cellulose nanocrystal flakes (CNCFs) as an effective dielectric to enhance generator performance and energy conversion efficiency. The sizes of bio-renewable cellulose nanocrystals were up-sized from nanospheres to micro flakes. Compared with a pure PDMS film, the positive charges on the embedded CNCFs induced an extra electric field to drive more electrons to transfer from the metal surface to the insulator surface according to the electron exchange mechanism of triboelectric charge generation. An increased surface charge fosters more induced charges to transfer through the external circuit while enhancing the electric output performance. The increased surface charge density could be attributed to the addition of CNCFs, which increased

the dielectric constant and improved the flexibility. The uniformly distributed CNCFs made it possible to fabricate cellulose composite triboelectric generators (CTGs, 1.5 cm × 1.5 cm) with a peak open-circuit voltage of 320 V, a closed-circuit current density of 5 μA cm^{-2}, and an output power of 1.65 mW (0.76 mW cm^{-2}), with an external resistance of 10 MΩ under a 40 N compressive force, resulting in a 10-fold power increase in comparison with triboelectric generators (TENGs) made of a pure PDMS film. The enhanced power of the CTGs was capable of instantaneously lighting up as many as 100 multicolor commercial LEDs. This simple and scalable technique provides a promising solution for developing large-scale and practical self-powered devices, and stimulating the development of green, high-performance triboelectric generators.

Acknowledgements

This project was supported by the USDA National Institute of Food and Agriculture Award (no. 2011-67009-20056). The authors would like to acknowledge Rick Reiner at the Forest Products Laboratory for preparing the cellulose nanocrystals. The first author also wishes to acknowledge the Wisconsin Institute for Discovery at the University of Wisconsin–Madison, the Guangdong Provincial Natural Science Foundation of China (2016A030313511) and the National Fundamental Research Funds for the Central Universities of China (no. 20152M056) for their financial support.

References

1 Z. L. Wang and J. H. Song, *Science*, 2006, **312**, 242.
2 X. Wang, J. Song, J. Liu and Z. L. Wang, *Science*, 2007, **316**, 102.
3 Y. Qin, X. Wang and Z. L. Wang, *Nature*, 2008, **451**, 809.
4 R. Yang, Y. Qin, L. Dai and Z. L. Wang, *Nat. Nanotechnol.*, 2009, **4**, 34.
5 K. S. Shin, T. Y. Kim, G. C. Yoon, M. K. Gupta, S. K. Kim, W. Seung, H. Kim, S. Kim, S. Kim and S. W. Kim, *Adv. Mater.*, 2014, **26**, 5619.
6 D. Kim, K. Y. Lee, M. K. Gupta, S. Majumder and S.-W. Kim, *Adv. Funct. Mater.*, 2014, **24**, 6949.
7 S. Wang, L. Lin and Z. L. Wang, *Nano Lett.*, 2012, **12**, 6339.
8 G. Zhu, Z. H. Lin, Q. Jing, P. Bai, C. Pan, Y. Yang, Y. Zhou and Z. L. Wang, *Nano Lett.*, 2013, **13**, 847.
9 J. Chen, G. Zhu, W. Yang, Q. Jing, P. Bai, Y. Yang, T. C. Hou and Z. L. Wang, *Adv. Mater.*, 2013, **25**, 6094.
10 S. Niu, Y. Liu, S. Wang, L. Lin, Y. S. Zhou, Y. Hu and Z. L. Wang, *Adv. Mater.*, 2013, **25**, 6184.
11 M. W. Williams, *AIP Adv.*, 2012, 2.
12 W. R. Harper, *Contact and frictional electrification*, Laplacian Press, Morgan Hill, Calif., 1998.
13 M. M. Apodaca, P. J. Wesson, K. J. Bishop, M. A. Ratner and B. A. Grzybowski, *Angew. Chem.*, 2010, **49**, 946.
14 H. T. Baytekin, B. Baytekin, J. T. Incorvati and B. A. Grzybowski, *Angew. Chem.*, 2012, **51**, 4843.
15 H. T. Baytekin, A. Z. Patashinski, M. Branicki, B. Baytekin, S. Soh and B. A. Grzybowski, *Science*, 2011, **333**, 308.
16 C. Zhang, T. Zhou, W. Tang, C. Han, L. Zhang and Z. L. Wang, *Adv. Energy Mater.*, 2014, **4**, 1301798.
17 H. Zhang, Y. Yang, X. Zhong, Y. Su, Y. Zhou, C. Hu and Z. L. Wang, *ACS Nano*, 2014, **8**, 680.
18 Y. Yang, G. Zhu, H. Zhang, J. Chen, X. Zhong, Z.-H. Lin, Y. Su, P. Bai, X. Wen and Z. L. Wang, *ACS Nano*, 2013, **7**, 9461.
19 X. Wen, W. Yang, Q. Jing and Z. L. Wang, *ACS Nano*, 2014, **8**, 7405.
20 Z. H. Lin, G. Cheng, W. Wu, K. C. Pradel and Z. L. Wang, *ACS Nano*, 2014, **8**, 6440.
21 W. Yang, J. Chen, G. Zhu, J. Yang, P. Bai, Y. Su, Q. Jing, X. Cao and Z. L. Wang, *ACS Nano*, 2013, **7**, 11317.
22 J. Chen, G. Zhu, J. Yang, Q. Jing, P. Bai, W. Yang, X. Qi, Y. Su and Z. L. Wang, *ACS Nano*, 2015, **9**, 105.
23 W. Seung, M. K. Gupta, K. Y. Lee, K.-S. Shin, J.-H. Lee, T. Y. Kim, S. Kim, J. Lin, J. H. Kim and S.-W. Kim, *ACS Nano*, 2015, **9**, 3501.
24 Z. L. Wang, J. Chen and L. Lin, *Energy Environ. Sci.*, 2015, **8**, 2250.
25 C. Zhang, J. Li, C. B. Han, L. M. Zhang, X. Y. Chen, L. D. Wang, G. F. Dong and Z. L. Wang, *Adv. Funct. Mater.*, 2015, **25**, 5625.
26 X. Wang, S. Wang, Y. Yang and Z. L. Wang, *ACS Nano*, 2015, **9**, 4553.
27 Q. Jing, Y. Xie, G. Zhu, R. P. Han and Z. L. Wang, *Nat. Commun.*, 2015, **6**, 8031.
28 Y. Jie, N. Wang, X. Cao, Y. Xu, T. Li, X. Zhang and Z. L. Wang, *ACS Nano*, 2015, **9**, 8376.
29 Z. Li, J. Chen, J. Yang, Y. Su, X. Fan, Y. Wu, C. Yu and Z. L. Wang, *Energy Environ. Sci.*, 2015, **8**, 887.
30 L. Lin, Y. Xie, S. Niu, S. Wang, P.-K. Yang and Z. L. Wang, *ACS Nano*, 2015, **9**, 922.
31 K. Y. Lee, J. Chun, J. H. Lee, K. N. Kim, N. R. Kang, J. Y. Kim, M. H. Kim, K. S. Shin, M. K. Gupta, J. M. Baik and S. W. Kim, *Adv. Mater.*, 2014, **26**, 5037.
32 S. Wang, Y. Zi, Y. S. Zhou, S. Li, F. Fan, L. Lin and Z. L. Wang, *J. Mater. Chem. A*, 2016, **4**, 3728.
33 Z. Lin, Y. Xie, Y. Yang, S. Wang, G. Zhu and Z. L. Wang, *ACS Nano*, 2003, **7**, 4554.
34 X. He, H. Guo, X. Yue, J. Gao, Y. Xi and C. Hu, *Nanoscale*, 2015, **7**, 1896.
35 J. Chun, J. W. Kim, W.-s. Jung, C.-Y. Kang, S.-W. Kim, Z. L. Wang and J. M. Baik, *Energy Environ. Sci.*, 2015, **8**, 3006.
36 Y. Zi, S. Niu, J. Wang, Z. Wen, W. Tang and Z. L. Wang, *Nat. Commun.*, 2015, **6**, 8376.
37 S. Wang, L. Lin, Y. Xie, Q. Jing, S. Niu and Z. L. Wang, *Nano Lett.*, 2013, **13**, 2226.
38 H. T. Baytekin, B. Baytekin, T. M. Hermans, B. Kowalczyk and B. A. Grzybowski, *Science*, 2013, **341**, 1368.
39 W. R. Harper, *Nature*, 1951, **167**, 400.

40 W. R. Harper, *Proc. R. Soc. London, Ser. A*, 1951, **205**, 83.
41 G. A. Cottrell, J. Lowell and A. C. Roseinnes, *J. Appl. Phys.*, 1980, **51**, 1250.
42 J. Lowell and A. C. Roseinnes, *Adv. Phys.*, 1980, **29**, 947.
43 P. Bai, G. Zhu, Y. S. Zhou, S. H. Wang, J. S. Ma, G. Zhang and Z. L. Wang, *Nano Res.*, 2014, **7**, 990.
44 Y. S. Zhou, S. Wang, Y. Yang, G. Zhu, S. Niu, Z. H. Lin, Y. Liu and Z. L. Wang, *Nano Lett.*, 2014, **14**, 1567.